INVESTIGATING IMPLICIT SHAPE REPRESENTATIONS FOR ALIGNMENT OF LIVERS FROM SERIAL CT EXAMINATIONS

Nathan D. Cahill[1,2], Grace Vesom[1], Lena Gorelick[3], Joanne Brady[4], J. Alison Noble[1], and J. Michael Brady[5]

[1]Institute of Biomedical Engineering, University of Oxford, Oxford OX3 HDQ, UK
[2]Research & Innovation, Carestream Health, Inc., Rochester, NY 14608, USA
[3]Computer Vision Group, The Weizmann Institute of Science, Rehovot 76100, Israel
[4]Department of Oncology, Churchill Hospital, Oxford OX3 7LJ, UK
[5]Wolfson Medical Vision Laboratory, University of Oxford, Oxford OX1 3PJ, UK

ABSTRACT

In this paper, we examine the use of implicit shape representations for nonrigid registration of serial CT liver examinations. Using ground truth in the form of corresponding landmarks manually labeled by a radiotherapist, we carry out an experiment to determine whether nonrigid registration performs better when applied to the original image data or to images constructed from implicit representations of the liver. We compare a variety of standard regularizers (elastic, diffusion, and curvature), similarity measures (sum of squared differences and mutual information), and weighting factors, using three different implicit shape representations: the Euclidean Distance Transform, the Poisson Transform (based on the expected hitting time of a random walk), and a new transform designed to highlight concavities in the shape.

Index Terms— Image registration, shape, biomedical imaging

1. INTRODUCTION

There are many ways to tackle the problem of image registration. One traditional classification of image registration approaches is into image-based or landmark-based approaches. Image-based registration involves the minimization of a function of the image values (such as the sum of squared differences (SSD) or mutual information (MI)) of the images being registered. Landmark-based registration involves minimizing a criterion that describes the geometric distance between features in two images. In the case of liver CT examinations, natural features would include points on the surface of the liver or the entire liver surface itself.

In recent years, a number of researchers have blurred the distinction between image-based and landmark-based approaches to registration. They have done so by constructing images from implicit representations of shapes, and then by performing image-based registration on the resulting images. The signed Euclidean Distance Transform (DT) is the most commonly used representation for shape registration [1, 2, 3], although Hong *et al.* [4] introduce a different representation called the *integral kernel*, which is related to the solution of the heat equation over a shape. The specifics of the registration algorithms differ: Paragios *et al.* [1] minimize a function related to SSD over the space of global rigid and local nonparametric deformations; Huang *et al.* [2] minimize MI over the space of free-form deformations parameterized by B-splines; Rosenhahn *et al.* [3] minimize the SSD within an optic flow estimation framework; and, Hong *et al.* [4] minimize SSD over the space of nonparametric deformations, subject to an elastic regularizer [5].

In this paper, we investigate the use of implicit shape representations for the nonrigid registration of serial CT examinations of the liver. We explore representations based on the signed distance transform and on the solution to Poisson's equation [6]. Using a set of CT liver examinations from a drug study, with manual liver segmentations approved by a clinician, we determine (a) whether nonrigid registration based on implicit representations of the liver outperforms nonrigid registration based on the original CT image data, and (b) the optimal choice of dissimilarity measure, regularizer, and weighting factor used by the nonrigid registration algorithm. To aid in answering these questions, we use sets of internal landmarks manually labeled by a radiotherapist as ground truth from which to measure target registration error (TRE).

2. PRELIMINARIES

2.1. Image Registration

Consider a reference image I_{ref} and a floating image I_{float}, both as functions in $\mathbf{R}^n$, and assume they have been globally aligned. Define a *deformation* $\mathbf{\Phi} : \mathbf{R}^n \mapsto \mathbf{R}^n$ by:

$$\mathbf{\Phi}(\mathbf{x}) = \mathbf{x} - \mathbf{u}(\mathbf{x}), \tag{1}$$

and call $\mathbf{u}$ the *displacement*.

The object of registration is to find a displacement that minimizes a dissimilarity measure D that measures the dissimilarity between I_{ref} and the deformed image $I^{\mathbf{u}}_{float} := I_{float}(\mathbf{\Phi})$. In order to ensure that the minimization problem is well-posed, a regularizing term R must be added to the dissimilarity measure. The general form of the registration problem is usually stated as:

$$\min_{\mathbf{u}} \quad D\big(I_{ref}, I^{\mathbf{u}}_{float}\big) + \alpha R(\mathbf{u}), \tag{2}$$

where α is a positive weighting factor.

The solution to (2) can be found by solving the corresponding *Euler-Lagrange equations*:

$$\begin{aligned} \alpha \mathbf{A}\mathbf{u}(\mathbf{x}) &= -\mathbf{f}(\mathbf{x}, \mathbf{u}(\mathbf{x})) \quad \forall \mathbf{x} \in \Omega, \\ \mathbf{B}[\mathbf{u}(\mathbf{x})] &= 0 \quad \forall \mathbf{x} \in \partial\Omega, \end{aligned} \tag{3}$$

where Ω is the interior of the domain $\bar{\Omega}$ over which the images are defined, $\partial\Omega = \bar{\Omega} - \Omega$ is the boundary of Ω, $\mathbf{A}$ is the partial differential operator and $\mathbf{f}$ the *force vector*, taken from the Gâteaux derivatives of R and D, respectively, and $\mathbf{B}$ is the boundary condition operator, which is typically chosen to enforce Dirichlet, Neumann, or periodic conditions on $\partial\Omega$.

Modersitzki [5] describes various homogeneous regularizers for use with nonparametric image registration. The partial differential operators corresponding to each of the standard regularizers are shown in Table 1. Modersitzki also presents the fluid regularizer,

Regularizer	Partial Differential Operator A
Elastic	$-\mu\Delta\mathbf{u} - (\lambda+\mu)\nabla\mathrm{div}\,\mathbf{u}$
Diffusion	$-\Delta\mathbf{u}$
Curvature	$\Delta^2\mathbf{u}$

Table 1. Standard homogeneous regularizers

which is equivalent in form to the elastic regularizer but is applied to the velocities of the deformation field. In practice, we have found that if displacement fields are updated in a memoryless fashion, the elastic and fluid regularizers yield very similar results.

A variety of dissimilarity measures have been developed for nonparametric registration; we focus on two: SSD and MI. SSD assumes that the only differences between values of registered images is due to Gaussian noise, whereas MI assumes a more flexible statistical relationship between the image values.

Numerical approximations to the stationary solution of (3) can be found by fixed-point iteration [5]. If R is one of the standard homogeneous regularizers and the boundary conditions are Dirichlet, then the partial differential operator is nonsingular and each iteration has a unique solution that can be found efficiently using Fourier methods [7].

2.2. Implicit Shape Representations

Let us define S to be the interior of the shape $\bar{S}$ and assume that $S \subset \Omega$. Then $\partial S = \bar{S} - S$ is the boundary of S.

2.2.1. Euclidean Distance Transform

The signed Euclidean Distance Transform (DT) W_{DT} yields two pieces of information: the magnitude provides the Euclidean distance between a point and the closest point on ∂S, and the sign provides an indicator as to whether the current point is inside S (positive) or outside S (negative). Mathematically speaking, W_{DT} is the solution to the Eikonal equation:

$$\begin{aligned} |W_{DT}(\mathbf{x})| &= 1 \quad \forall \mathbf{x} \in S, \\ W_{DT}(\mathbf{x}) &= 0 \quad \forall \mathbf{x} \in \partial S. \end{aligned} \tag{4}$$

Fig.'s 1(a) and 1(a) show a segmented liver and orthogonal slices of the DT of that liver.

2.2.2. Poisson Transform

Gorelick *et al.* [6] presented an implicit shape representation based on the expected time for a symmetric random walk to reach the shape boundary. Based on the solution to Poisson's equation, this representation was shown to have superior behavior over the DT for shape classification, due to its differentiability and its smoothing of noisy shape boundaries. When extended to three dimensions and assigned a negative sign on the shape interior, this *Poisson Transform* (PT) W_{PT} satisfies

$$\begin{aligned} \Delta W_{PT}(\mathbf{x}) &= 6 \quad \forall \mathbf{x} \in S, \\ W_{PT}(\mathbf{x}) &= 0 \quad \forall \mathbf{x} \in \partial S. \end{aligned} \tag{5}$$

On the exterior of the shape, if no further boundary conditions are prescribed, the random-walk analogy fails, and the Poisson equation has infinitely many solutions. Therefore, in order to provide an extension of this shape representation to the entirety of $\bar{\Omega}$, we need to define some sort of external boundary condition. One option is to enforce Neumann boundary conditions on $\partial\Omega$; however, this yields undesirable behavior of the PT gradient at the image boundaries. Instead, we define an open sphere $T \supset \bar{\Omega}$ centered on the centroid of Ω, and solve the following boundary value problem:

$$\begin{aligned} \Delta W_{PT}(\mathbf{x}) &= -6 \quad \forall \mathbf{x} \in T - \bar{S}, \\ \langle \nabla W_P(\mathbf{x}), \vec{\mathbf{n}}(\mathbf{x}) \rangle &= 0 \quad \forall \mathbf{x} \in \partial T, \\ W_{PT}(\mathbf{x}) &= 0 \quad \forall \mathbf{x} \in \partial S, \end{aligned} \tag{6}$$

where $\vec{\mathbf{n}}(\mathbf{x})$ is the outward-pointing normal vector to the surface ∂T at $\mathbf{x}$. The Neumann boundary condition on ∂T effectively reflects the symmetric random walk in the direction normal to the sphere. Once W_{PT} has been found on T, it can be cropped to the original image domain $\bar{\Omega}$.

Computing a discrete approximation of W_{PT} inside S can be done in linear time with the multigrid algorithm described in [6, 8]. This algorithm can be extended to approximate W_{PT} inside $T - \bar{S}$ by appropriately discretizing the Neumann boundary conditions. We have found that applying two w-cycles, which employ naive boundary conditions at the coarse levels (placing the boundary at the nearest coarse grid points, instead of modifying the nearby coarse equations to account for the fine, pixel-level location of the boundary), yields a good approximation.

Fig. 1(c) shows orthogonal slices of a version of the PT that has been chosen to enhance contour visualization.

2.2.3. Ψ Transform

In addition to presenting the PT, Gorelick *et al.* [6] presented a function (in their Eq. (8)) based on the PT that proved to be very useful in detecting shape concavities. In order to investigate its potential usefulness for registration, we generalize her original Φ function to both the interior and exterior of a shape in 3D, and relabel the function Ψ in order to avoid any confusion with the deformation in (1):

$$\Psi(\mathbf{x}) = \begin{cases} W_{PT}(\mathbf{x}) - \frac{1}{4}\left\|\nabla W_{PT}(\mathbf{x})\right\|^2, & \forall \mathbf{x} \in \bar{S} \\ W_{PT}(\mathbf{x}) + \frac{1}{4}\left\|\nabla W_{PT}(\mathbf{x})\right\|^2, & \forall \mathbf{x} \notin \bar{S}. \end{cases} \tag{7}$$

We define the Ψ *Transform* (ΨT) by:

$$W_\Psi(\mathbf{x}) = \begin{cases} \ln(1 - \Psi(\mathbf{x})), & \forall \mathbf{x} \in \bar{S} \\ \ln(1 + \Psi(\mathbf{x})), & \forall \mathbf{x} \notin \bar{S}. \end{cases} \tag{8}$$

Note that the W_Ψ is continuous everywhere except on ∂S, due to the differentiability of W_{PT}. Fig. 1(d) shows orthogonal slices of ΨT.

3. REGISTRATION EXPERIMENT

In order to determine whether implicit shape representations are useful for nonrigid registration of livers, we designed an experiment using a data set of serial CT liver scans. The data set was taken from

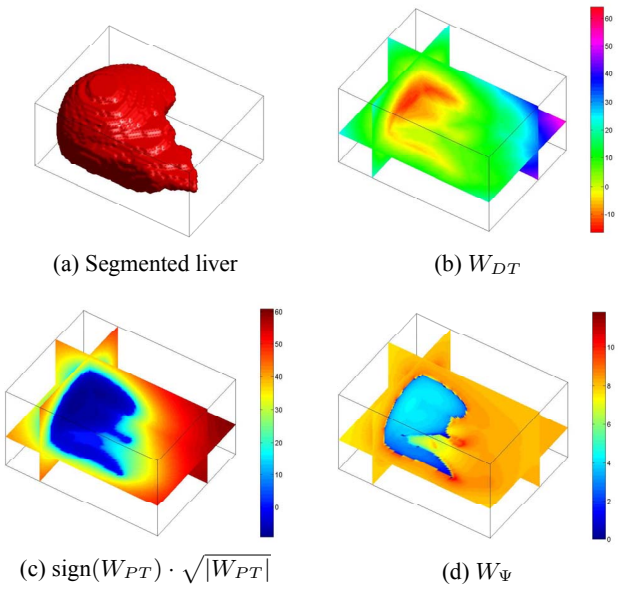

(a) Segmented liver (b) W_{DT}

(c) $\text{sign}(W_{PT}) \cdot \sqrt{|W_{PT}|}$ (d) W_{Ψ}

Fig. 1. Segmented liver and implicit shape representations.

a drug trial where serial scans were done for each patient to monitor tumours undergoing an experimental treatment for colorectal metastases in the liver. Five patients were randomly chosen, and their first and last scans form image pairs to be registered. All scans are spiral CT scans with voxel size $1 \times 1 \times 7.5$ mm^3, with the exception of one scan with voxel size $1 \times 1 \times 5$ mm^3. Liver delineation was done manually on a slice-by-slice basis and approved by a clinician.

A set of 4-8 corresponding landmarks that were used as ground truth for validation were chosen in each image pair by a radiotherapist. The landmarks were based on target points visible on both scans, and were the locations of vascular or ductal branching points or hepatic fissures.

To reduce the amount of computational overhead, we resampled each image to a resolution of $4 \times 4 \times 4$ mm^3, yielding volumetric images on the order of $128 \times 128 \times 25$ voxels. Affine alignment via optimal linear registration was performed to align each of the image pairs, as well as to align binary images of the liver segments derived from each pair. From the affine-aligned images, we computed DT, PT, and ΨT. For each type of image pair of affine-aligned images (original, DT, PT, and ΨT), we nonrigidly registered the current scan to the prior scan using nonparametric deformation fields with Dirichlet boundary conditions, while varying the following parameters:

- Dissimilarity Measure: {SSD, MI}
- Regularizer: {Elastic, Diffusion, Curvature}
- Weighting Factor α: {0.1, 1, 10, 100}

Note that for the original images, we did not consider MI as a dissimilarity measure, given that each original image in a pair was from the same modality and of the same patient.

For each resulting deformation field, we predicted where each current ground truth landmark would have come from in the prior scan. From these predicted positions and the known positions of the landmarks in the prior scans, we computed the mean Target Registration Error (TRE) in millimeters. Optimal weighting factors were found for each combination of image type, dissimilarity measure and regularizer, by choosing the weighting factor in which TRE was reduced the most.

4. RESULTS

Table 2 illustrates the best weighting factors found for each combination of the other parameters. The first and second numbers in each entry correspond to the use of the SSD and MI dissimilarity measures, respectively.

Regularizer	Original	DT	PT	Ψ
Elastic	100/NA	1/10	100/100	0.1/1
Diffusion	1/NA	0.1/1	0.1/10	0.1/0.1
Curvature	10/NA	0.1/0.1	10/0.1	10/0.1

Table 2. Optimal weighting factor α, (SSD/MI); NA = not applicable

Fig. 2 shows the mean TRE (in millimeters) for each type of registration performed on each patient, with the optimal weighting factors taken from Table 2.

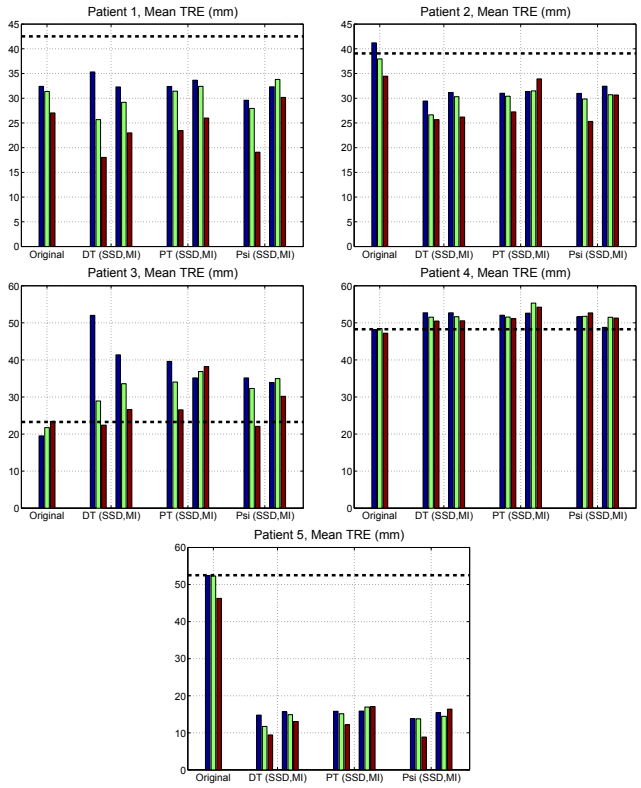

Fig. 2. Mean TRE results for each patient, using elastic (blue), diffusion (green), and curvature (red) regularizers. The horizontal, dashed line indicates the TRE computed without any registration.

Some general conclusions can be drawn from these results. First, none of the nonrigid registration algorithms appeared to perform well on patients 3 and 4, regardless of whether they were based on the original images or on implicit representations of the liver. To

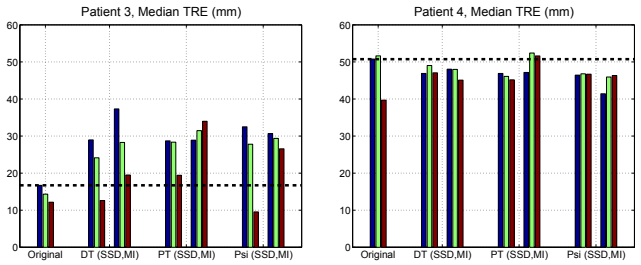

Fig. 3. Median TRE results patients 3 and 4, using elastic (blue), diffusion (green), and curvature (red) regularizers.

investigate the potential problems, we show the median TRE values for these patients in Fig. 3. From this additional information, it is clear that for patient 3, the only possibility for slight improvement in TRE lies in the use of the curvature regularizer applied to the original, DT, or ΨT images. For patient 4, the lower median TRE values show that some of the landmarks are being moved slightly closer due to nonrigid registration, but one or more of the landmarks might be outliers.

Based on the remaining patients, the diffusion and curvature regularizers generally perform better when minimizing SSD than when minimizing MI. In addition, the curvature regularizer generally outperforms the diffusion and elastic regularizers when SSD is minimized. It is clear from these results that, independent of whether the registration is based on the original images or on some implicit shape representation, the use of the curvature regularizer in conjunction with SSD is preferred.

With this combination of curvature/SSD, it is also clear that registration based on any of the implicit shape representations outperforms registration based on the original image data. Furthermore, the DT and ΨT images appear to slightly outperform the PT images.

5. DISCUSSION

This experiment provides insight into the applicability of nonrigid registration techniques in clinical practice. First, the validation with manually labeled ground truth yielded surprising results. In two of the five patients, nonrigid registration failed to provide any noticeable improvement in TRE over no registration at all, even though the SSD and MI dissimilarity measures were suitably reduced/enhanced. Furthermore, in only one of the remaining three patients did the mean TRE approach 1 centimeter. This could be due to errors in the manually labelled landmarks, although it does suggests that robust subcentimeter accurate nonrigid registration of livers is still an open problem.

The relatively outstanding performance of the curvature regularizer over the diffusion and elastic regularizers was also an interesting result, given that it might seem that elastic regularizers could be readily tuned via biomechanical models of the underlying tissue. One possible explanation is that the curvature regularizer has a much broader Green's function than the diffusion or elastic regularizers. This could equate to smoother overall deformations in practice.

Finally, it was somewhat surprising to see that the use of the PT yielded slightly worse results than the use of the DT. We had expected the opposite result, given the PT's differentiability and better ability to quickly become smooth around noisy surfaces. One possible explanation is that the points of nondifferentiability in the DT were more salient than any points in the PT, giving the force fields larger weight in those areas. However, the comparable performance of the ΨT to the DT is also interesting, given that the ΨT is a function of the PT itself. This suggests that there may be further information that can be gleaned from the PT that might be more useful for registration.

6. CONCLUSIONS AND FUTURE WORK

In this paper, we used serial CT examinations of the liver to examine the use of implicit shape representations for nonrigid registration. Using ground truth in the form of corresponding landmarks manually labeled by a radiotherapist, we were able to make the following conclusions. First, in some cases, global + nonrigid registration fails to perform better than using no registration at all. Second, in cases where nonrigid registration does yield a clinicial improvement, the use of implicit representations of the liver outperforms the use of the original image data. Third, in these cases, the use of the standard curvature regularizer and sum of squared differences dissimilarity measure is preferred over other standard regularizers, and over mutual information.

There are many potential areas for exploration, such as: the use of other features derived from the DT or PT; the use of scale-space shape representations; the fusion of shape and texture information for registration; the use of inverse-consistent registration techniques; and, the robustness of these registration techniques to various automatic (imperfect) segmentations of the liver.

7. ACKNOWLEDGEMENTS

The authors thank Prof. David Hawkes of the Centre for Medical Image Computing at the University College London for helpful discussions on nonrigid registration.

8. REFERENCES

[1] N. Paragios, M. Rousson, and V. Ramesh, "Non-rigid registration using distance functions," *CVIU*, vol. 89, no. 2-3, pp. 142–165, 2003.

[2] X. Huang, N. Paragios, and D. N. Metaxas, "Shape registration in implicit spaces using information theory and free form deformations," *IEEE Trans. PAMI*, vol. 28, no. 8, pp. 1303–1318, August 2006.

[3] B. Rosenhahn, T. Brox, D. Cremers, and H.-P. Seidel, "A comparison of shape matching methods for contour based pose estimation," *Comb. Image Anal.*, vol. LNCS 4040, pp. 263–276, 2006.

[4] B.-W. Hong, E. Prados, S. Soatto, and L. Vese, "Shape representation based on integral kernels: Application to image matching and segmentation," in *Proc. CVPR*, 2006, pp. I: 833–840.

[5] J. Modersitzki, *Numerical Methods for Image Registration*, Oxford University Press, 2004.

[6] L. Gorelick, M. Galun, E. Sharon, R. Basri, and A. Brandt, "Shape representation and classification using the Poisson equation," *IEEE Trans. PAMI*, vol. 28, no. 12, pp. 1991–2005, December 2006.

[7] N. D. Cahill, J. A. Noble, and D. J. Hawkes, "Fourier methods for nonparametric image registration," *Proc. CVPR*, pp. 1–8, 2007.

[8] U. Trottenberg, C. W. Oosterlee, and Schüller, *Multigrid*, Academic Press, 2001.